Comparison of self-processing of foot-and-mouth disease virus leader proteinase and porcine reproductive and respiratory syndrome virus leader proteinase nsp1α ☆

Jutta Steinberger [a], Georg Kontaxis [b], Chiara Rancan [c], Tim Skern [a,*]

[a] Max F. Perutz Laboratories, Medical University of Vienna, Department of Medical Biochemistry, Dr. Bohr-Gasse 9/3, A-1030 Vienna, Austria
[b] Max F. Perutz Laboratories, University of Vienna, Department of Structural and Computational Biology, Campus Vienna Biocenter 5, A-1030 Vienna, Austria
[c] Helmholtz Zentrum München, Department of Gene Vectors, Haematologikum, Marchioninistrasse 25, D-81377 Munich, Germany

ARTICLE INFO

ABSTRACT

The foot-and-mouth disease virus leader proteinase (Lb[pro]) cleaves itself off the nascent viral polyprotein. NMR studies on the monomeric variant Lb[pro] L200F provide structural evidence for intramolecular self-processing. ^{15}N-HSQC measurements of Lb[pro] L200F showed specifically shifted backbone signals in the active and substrate binding sites compared to the monomeric variant sLb[pro], lacking six C-terminal residues. This indicates transient intramolecular interactions between the C-terminal extension (CTE) of one molecule and its own active site. Contrastingly, the porcine reproductive and respiratory syndrome virus (PRRSV) leader proteinase nsp1α, with a papain-like fold like Lb[pro], stably binds its own CTE. Parts of the β-sheet domains but none of the α-helical domains of Lb[pro] and nsp1α superimpose; consequently, the α-helical domain of nsp1α is oriented differently relative to its β-sheet domain. This provides a large interaction surface for the CTE with the globular domain, stabilising the intramolecular complex. Consequently, self-processing inactivates nsp1α but not Lb[pro].

© 2013 The Authors. Published by Elsevier Inc. All rights reserved.

Introduction

Many viral proteinases have been proposed to cleave themselves from their respective polyproteins in an intramolecular manner. However, structural evidence and insights into the mechanism of intramolecular self-processing of viral proteinases are sparse (Tang et al., 2008). Two important exceptions are the papain-like cysteine proteinases of PRRSV, termed nsp1α and nsp1β; structures of both enzymes determined by X-ray crystallography show that extensions to the C-terminus (CTE, C-terminal extension) of the papain-like fold reach back into the globular domain and bind intramolecularly into the active site (Sun et al., 2009; Xue et al., 2010). Furthermore, for both enzymes, the CTE is bound in a stable manner, suggesting that the mature enzyme is not active after self-processing.

In contrast, the mature leader proteinase (Lb[pro]) of foot-and-mouth disease virus (FMDV) is active after self-processing, as it performs rapid cleavage of the host protein eukaryotic initiation factor (eIF) 4G (Devaney et al., 1988). This indicates that the CTE of the Lb[pro] cannot remain permanently and irreversibly bound to the active site. Previous attempts to analyse the nature of the interaction of Lb[pro] with its CTE have been hampered by the tendency of wild-type (wt) Lb[pro] to form a strong homodimer, both in the crystal and in solution (Cencic et al., 2007; Guarne et al., 1998). In these homo-dimers, the C-terminal seven residues of the 18 amino acid long CTE specifically bind to the substrate binding site of the adjacent molecule and vice versa (Santos et al., 2009). This arrangement would argue for an intermolecular (trans) mechanism of self-cleavage. However, the kinetics of processing observed with Lb[pro] containing proteins synthesised from viral sub-genomic mRNAs in rabbit reticulocyte lysates has provided strong in vitro evidence that the reaction is indeed an intramolecular one (Glaser et al., 2001).

The structural investigation of intramolecular Lb[pro] self-processing thus requires the generation of a variant that remains monomeric but still contains a full-length CTE. As an approach to generate such a monomeric form, we decided to examine a mutant of Lb[pro] whose activity is severely reduced in self-processing through the substitution of Leu 200, the penultimate amino acid of the CTE, with Phe. It has been shown that the aromatic Phe side-chain is not well accepted in the S$_2$ pocket

* Corresponding author. Fax: +43 1 4277 9616.
E-mail address: timothy.skern@meduniwien.ac.at (T. Skern).

because of its size (Mayer et al., 2008). Consequently, we reasoned that the L200F mutation might perturb dimer formation and favor the formation of monomeric Lb^{pro} molecules. However, using the techniques of NMR, it should still be feasible to detect intramolecular interactions of the CTE with the substrate binding site.

We show here that the single mutation L200F is indeed sufficient to disrupt the stable dimer formation of wild-type Lb^{pro} and that an intramolecular mechanism underlies FMDV Lb^{pro} self-processing. Furthermore, we then compare the arrangements of the folds of Lb^{pro} and nsp1α relative to their CTE to demonstrate why the nsp1α can form a stable intramolecular complex with its CTE whereas the Lb^{pro} cannot.

Materials and methods

Materials

$^{13}C_6$-D-glucose was purchased from Sigma-Aldrich, Germany, and ^{15}N-ammonium chloride was purchased from Euriso-Top, France.

The bacterial expression plasmids Lb^{pro} C51A (FMDV residues 29–201) and sLb^{pro} C51A (FMDV residues 29–195) have previously been described (Guarne et al., 1998). The mutation L200F was introduced into pET11d Lb^{pro} C51A via site-directed PCR mutagenesis. The encoded proteinases lack the catalytic cysteine residue C51 and are thus proteolytically inactive, ensuring long-term sample stability.

Protein expression, purification and analytical size-exclusion chromatography

Proteins were expressed in BL21(DE3)pLysS bacteria grown in LB-medium for size-exclusion chromatography or minimal medium containing $^{13}C_6$-D-glucose as the sole carbon source and ^{15}N-ammonium chloride as the sole nitrogen source for NMR studies.

Expression and purification of Lb^{pro} was performed as described (Cencic et al., 2007) with the following modifications. Transformed bacteria were grown in M9 medium overnight. Protein expression was induced at an OD_{600} between 0.5 and 0.6 and continued for 17 h. After ammonium sulphate precipitation, the protein sample was dialysed against two liters of Buffer A (Cencic et al., 2007). Furthermore, anion-exchange chromatography was performed on a Mono Q HR 10/10 column (GE Healthcare). For preparative size-exclusion chromatography, a HiLoad 26/60 Superdex 75 pg column was used (GE Healthcare). For NMR experiments, the buffer of the protein solution was changed from buffer A to NMR buffer (20 mM sodium phosphate pH 7.0, 50 mM NaCl, 5 mM DTT) via dialysis. In addition, the sample was concentrated to between 0.5 and 2 mM using Amicon Ultra Centrifugal Devices with a 10 kDa cut-off (Millipore). NMR samples also contained 5–10% (v/v) ^2H_2O for field-frequency lock.

To express unlabelled Lb^{pro} for analytical gel-filtration experiments, E. coli BL21(DE3)pLysS bacteria were transformed with the respective Lb^{pro} variant and grown in LB-medium overnight. The starter culture was diluted 1:10 (v/v) in LB-medium. The rest of the expression and purification protocol was performed as described above, except that the expression temperature was 30 °C.

For analytical size-exclusion chromatography 1.5 mg of the standard proteins ovalbumin (43 kDa), chymotrypsinogen A (25 kDa) and ribonuclease A (13.7 kDa) of the Gel Filtration Calibration Kit LMW (GE Healthcare) were used, whereas 0.5 mg of the Lb^{pro} variant were used. Analysis was performed on a HiLoad 16/60 Superdex 75 prep grade column (GE Healthcare) as described previously (Cencic et al., 2007).

NMR spectroscopy

^{15}N-HSQC experiments, ^{15}N T_2 measurements and 3D triple resonance experiments (using $^{15}N/^{13}C$ labelling, when required for

signal assignment) were performed on a Varian/Agilent DirectDrive 600 MHz spectrometer as described in (Cencic et al., 2007). Spectra were processed using NMRPipe (Delaglio et al., 1995) and analyzed using Sparky (Goddard and Kneller) software.

Chemical shift changes were calculated as weighted averages 1H and 15 N chemical shift differences according to $\Delta\sigma = \{\Delta\sigma(^{15}N)^2 + [5\Delta\sigma(^1H)]^2\}^{1/2}$.

Molecular modelling

Structural alignments and superimpositions were done using the DALI server (Holm and Sander, 1993). All drawings were
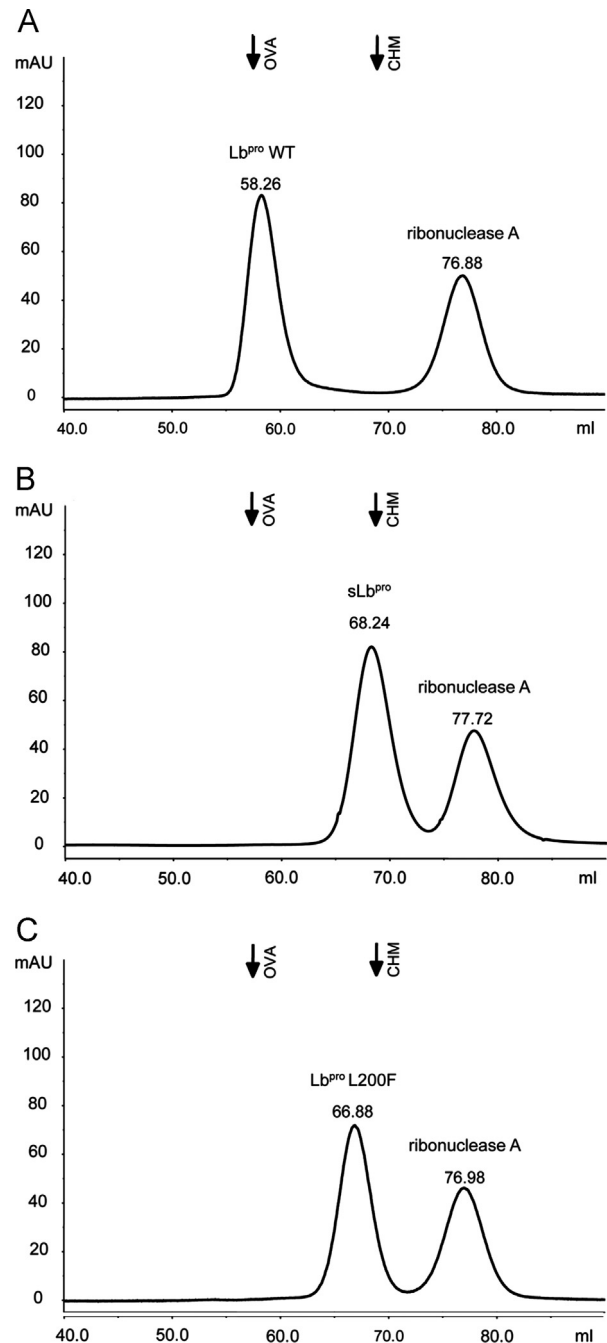
Fig. 1. Oligomerisation states of Lb^{pro} variants. The oligomerisation state of wt Lb^{pro} (A), sLb^{pro} (B) and Lb^{pro} L200F (C) were analysed via size-exclusion chromatography on a HiLoad 16/60 Superdex 75 prep grade column together with ribonuclease A (13.7 kDa) as an internal standard. 0.5 mg of wt Lb^{pro} or the variants were analysed together with 1.5 mg of ribonuclease A. Positions of the standard proteins ovalbumin (OVA, 43 kDa) and chymotrypsinogen A (CHM, 25 kDa) are indicated.

created using PYMOL(DeLano, 2002). The PDB identifiers of the structures used were 1QOL for Lb^pro and 3IFU for the PRRSV nsp1α.

Results

Wild-type Lb^pro has been shown in both the crystal and in solution to behave as a dimer (Cencic et al., 2007; Guarne et al., 2000). Dimerisation occurs through the interaction of the CTE of one molecule and the substrate binding region of the neighbouring one and vice versa. Lb^pro monomers can be most easily prepared by deletion of the last six amino acids of the CTE to give sLb^pro (shortened Lb^pro), thus preventing dimer formation (Guarne et al., 2000). However, this form clearly cannot provide any information on the interaction of the CTE with the active site. In the search for a monomeric form of Lb^pro that still allows an interaction of the CTE with the active site, we noted that the variant Lb^pro L200F is impaired in but still allows self-processing (Kuehnel et al., 2004). This implies a reduced affinity of the enzyme for the CTE and consequently suggests that the interactions involved in dimer stability might also be reduced.

To this end, we decided to investigate further the oligomerisation state of Lb^pro L200F by size-exclusion chromatography. Wild-type (wt) Lb^pro and sLb^pro served as reference proteins for the dimeric and the monomeric states of Lb^pro, respectively, (Cencic et al., 2007). Fig. 1 shows the elution profiles of three investigated proteinases. Dimeric wt Lb^pro elutes at 58.26 ml, corresponding to a molecular weight of about 41.4 kDa (Fig. 1A). In contrast, the monomeric sLb^pro elutes at about 68.24 ml, corresponding to a molecular weight of about 28.8 kDa (Fig. 1B). The observed molecular weight of sLb^pro determined by size-exclusion chromatography is larger than its calculated molecular weight of 19.1 kDa. This presumably results from the presence of the unbound flexible CTE that extends away from the globular domain into the solution and thus results in a larger apparent particle dimension and effective molecular weight.

We next examined the variant Lb^pro L200F which eluted at an elution volume of 66.88 ml, indicating an observed apparent molecular weight of about 28.5 kDa, corresponding almost exactly to the elution profile of sLb^pro (Fig. 1C). To confirm that Lb^pro L200F is indeed a monomer, we used NMR to compare its ^{15}N T_2 transverse relaxation times with those of wt Lb^pro and sLb^pro. These parameters are indicative of the hydrodynamic properties and thus the effective molecular weight of the examined proteins. Fig. 2 shows that the ^{15}N T_2 relaxation times of Lb^pro L200F are indeed similar to those of sLb^pro (Fig. 2A) and about twice as long as those of wt Lb^pro (Fig. 2B). These data provide further evidence that Lb^pro L200F behaves as a

monomer in solution, in contrast to the wild-type Lb^pro which behaves as a dimer. The flexible CTE of Lb^pro L200F is reflected in its ^{15}N T_2 relaxation times being substantially longer than those of the globular domain. However, presumably due to spectral overlap even in 3D-triple resonance spectra in combination with dynamic exchange broadening, it was not possible to observe and assign signals for the last 12 residues of the wt Lb^pro or Lb^pro L200F.

The behaviour of Lb^pro L200F as a monomer allowed us to investigate some aspects of the intramolecular interaction of the CTE with the globular domain of the protein. To this end, Lb^pro L200F was labelled with ^{13}C and ^{15}N, purified, analysed and assigned by 3D triple resonance experiments.

Unfortunately, not all backbone ^{15}N–^1H signals of Lb^pro L200F could be assigned possibly due to exchange broadening, as mentioned above. In particular, backbone ^{15}N–^1H signals for the last 12 residues (190–201) of the CTE were missing, presumably due to fast relaxation. Such behaviour is usually indicative for dynamic phenomena occurring in the microseconds to milliseconds time regime. Generally speaking, exchange dynamics can have differential effects on relaxation behaviour depending on the timescale at which it occurs.

Being unable to directly observe signals for the last 12 residues of the C-terminus (residues 190 to 201) of the Lb^pro L200F variant, we could therefore gain no direct structural and dynamic information on this part of the CTE. The lack of observable signals could however indicate that there are transient interactions between the C-terminus and the substrate binding site in the intermediate time scale of milliseconds to microseconds. This would broaden the signals of these residues and render them undetectable.

If the CTE were conformationally completely unrestricted, as in the shortened deletion mutant sLb^pro, it would undergo extremely fast (micro- to nanoseconds) dynamics and its resonances would be consequently sharp and intense. In the other extreme, if such an interaction were to take place in a time period slower than the millisecond range, two separately observable signals for each residue, one for the bound and one for the unbound state, can be envisaged. Interestingly, this was the case for the ^{13}C $C\alpha$ signals of residues Glu 186 and Leu 188. This observation was at least partly explained as they are in the immediate vicinity of Pro 187, a residue conserved in all presently sequenced FMDV Lb^pro, indicating that Pro 187 may have a critical role in the structure and function of the C-terminus. This may be an indication that proline cis–trans isomerisation may, for example, contribute to the dynamic process(es) governing the behaviour of the CTE.

An overlay of the ^{15}N-HSQC spectra of Lb^pro L200F (red) and sLb^pro (black) (Cencic et al., 2007) is shown in Fig. 3A. The spectra
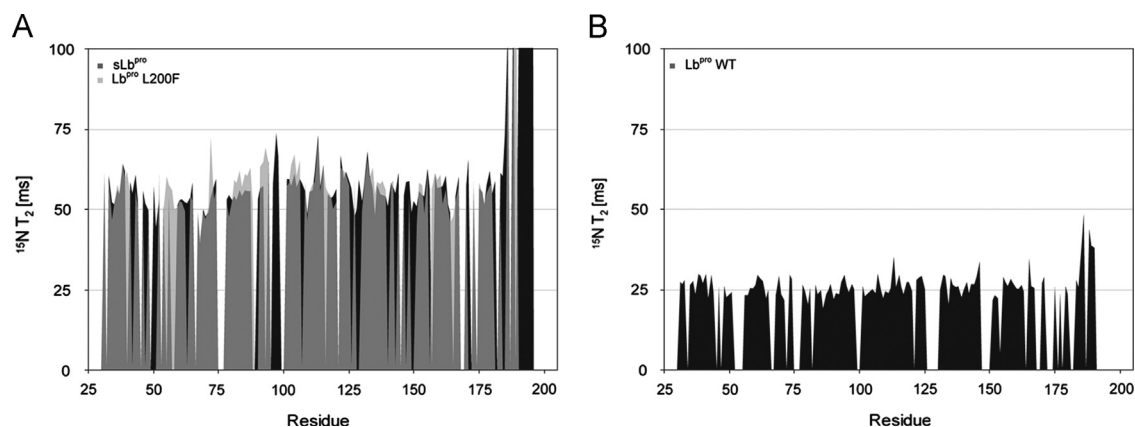
Fig. 2. ^{15}N T_2 transverse relaxation times of Lb^pro variants. (A) The relaxation times of sLb^pro (black) are almost identical to those of Lb^pro L200F (grey) confirming the monomeric state of Lb^pro L200F. (B) The relaxation times of wt Lb^pro (black) are roughly only half of those compared with sLb^pro and Lb^pro L200F, reflecting the presence of a dimer.
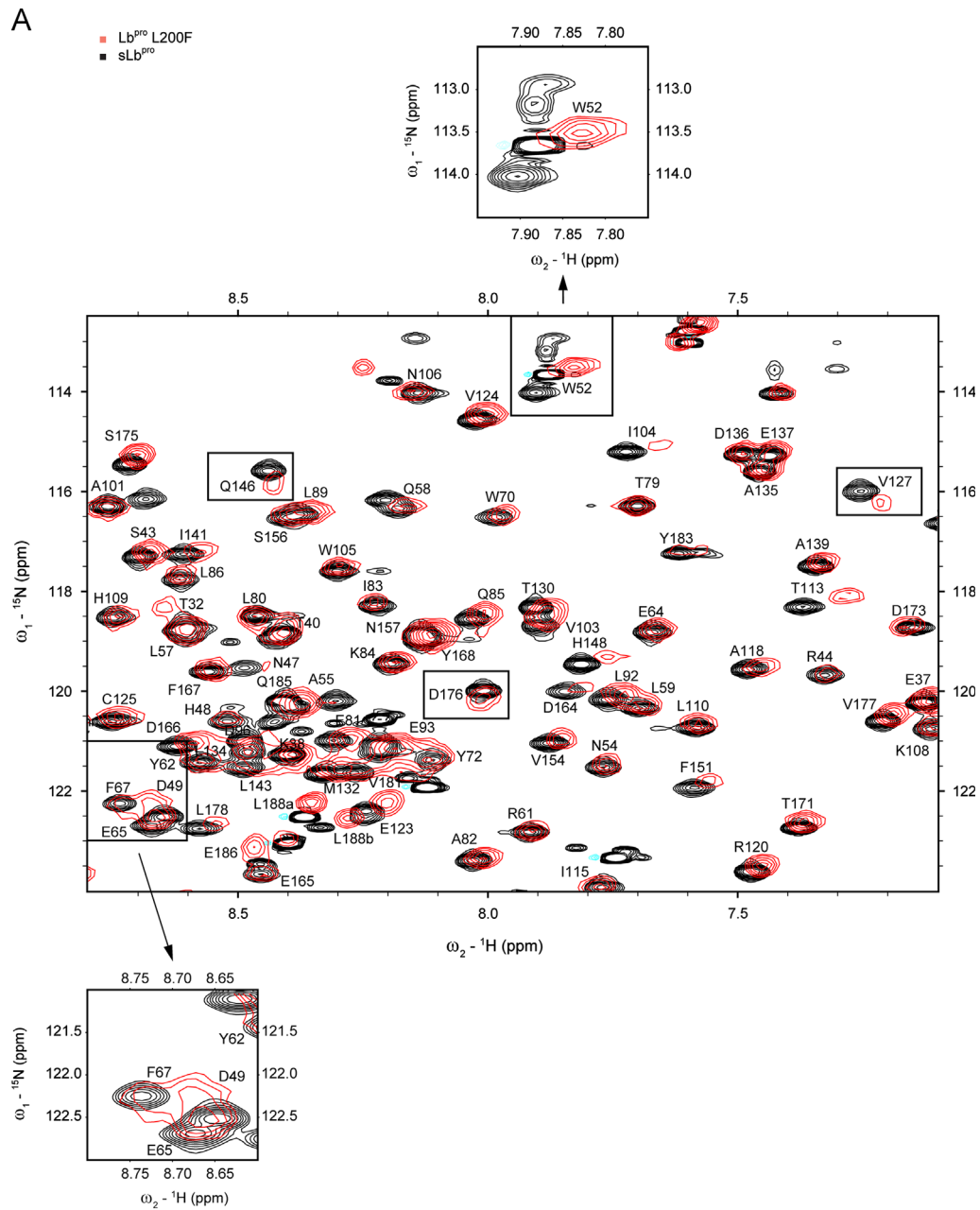
Fig. 3. Backbone Amide Shift differences between sLb[pro] and Lb[pro] L200F. (A) Overlaid ^{15}N HSQC spectra of sLb[pro] (black) and Lb[pro] L200F (red). The two spectra show an excellent mutual agreement. However, some signals are shifted, indicating distinct structural changes of Lb[pro] L200F. Residues that show shift differences higher than 0.50 ppm are highlighted by boxes; these include D49 (0.60 ppm), W52 (0.56 ppm), V127 (0.53 ppm), Q146 (0.70 ppm) and D176 (0.55 ppm). (B) Amide chemical shifts of sLb[pro] compared to Lb[pro] L200F. The $[\{5\Delta\sigma\,(^1H)\}^2+\{\Delta\sigma\,(^{15}N)\}^2]^{1/2}$ relationship was used to calculate amide resonance shifts in the ^{15}N HSQC spectra of Lb[pro] L200F. (For interpretation of the references to color in this figure legend, the reader is referred to the web version of this article.)

correlate to a very high extent, as the majority of the signals show either no or only minor ^{15}N–^1H shift differences (Fig. 3B). Nevertheless, distinct residues do have appreciable shift differences exceeding 0.50 ppm (see Materials and methods). These include Asp 49 (0.60 ppm), Trp 52 (0.56 ppm), Val 127 (0.53 ppm), Gln 146 (0.70 ppm) and Asp 176 (0.55 ppm), shown in boxes in Fig. 3A.

Residues of Lb^{pro} L200F that showed differences in signal shifts in the ^{15}N HSQC spectral comparison from those of sLb^{pro} were mapped onto the structure of a single molecule of the Lb^{pro} dimer (Fig. 4). The chemical shift changes were colour-coded according to their degree of difference ranging from low (0 ppm, blue) through medium (purple) to high (> 0.50 ppm, red). Interestingly, the signals that show the greatest shift differences largely map to residues that are located in the substrate binding cleft. No signals could be detected for the Ala 51 (substituting for active site nucleophile residue Cys 51). However, the flanking residues Asp 49 and Trp 52 displayed the greatest changes within the active site region of 0.60 and 0.56 ppm, respectively. In addition, signals in the loop connecting the β-strands β5 and β6 containing the active site residue His 148 could also not be detected. Within this loop, Gln 146, which is also involved in the formation of the S$_4$ subsite (Santos et al., 2009), shows the greatest shift difference measured of 0.70 ppm. Indeed, only a few other signals could be detected from residues that are involved in the formation of substrate binding sites. Signals from all of the residues building the S$_1$ subsites were lacking completely (His 95, Asp 96 and Asp 147). Of the ten amino acids that build the S$_2$ hydrophobic pocket accepting P$_2$ leucine, only four could be detected. Three showed reasonable to significant shift changes (Leu 178: 0.10, His 148: 0.40 and Trp 52: 0.56 ppm). Glu 93, the only one of the four amino acids building the S$_3$ subsite that could be detected, showed a moderate shift difference of 0.14 ppm. As mentioned above, the only signal that could be detected from a residue of the S$_4$ subsite was Gln 146, with the 0.70 ppm shift difference. No signals were detectable from residues of the S$_5$ subsite. The S$_6$ subsite is formed by four amino acids, of which only signals of three could be detected (Leu 178: 0.10, Val 127: 0.53 and Ala 101: 0.26 ppm). Finally, all signals arising from the surface located residues of helix α4 appear to be

affected (Fig. 4A), again indicating some transient interaction of the CTE with the globular domain.

Discussion

Here, we used the mutant Lb^{pro} L200F to investigate the molecular basis of Lb^{pro} dimerisation and intramolecular self processing. The analysis of Lb^{pro} L200F via size-exclusion chromatography (Fig. 1) as well as by NMR using the ^{15}N T$_2$ transverse relaxation times (Fig. 2) confirmed that Lb^{pro} L200F exists as a monomer in solution. This suggests that the dimer observed in the wild-type is exclusively stabilised by the interactions between the CTE and the active site. The K_D for the interaction between the CTE and the active site can be estimated to be in the mM range by NMR titration of the sLb^{pro} form with suitable CTE peptides. As the Lb^{pro} dimer is stabilized by *two* such interactions the resulting K_D of the dimer is thus better than μM (Cencic et al., 2007). Thus, a single mutation of Leu 200 to Phe is sufficient to disrupt the dimer.

A comparison of the ^{15}N HSQC spectra of Lb^{pro} L200F and sLb^{pro} showed that the majority of the signals are unaffected, arguing for overall unchanged protein structures and oligomerisation states. However, distinct signals were shifted, demonstrating changes of the chemical environment of certain residues. As Lb^{pro} L200F is present as a monomer, we infer that these alterations can only arise from the transient intramolecular interaction between the highly flexible CTE and the active site of the same molecule; an intermolecular interaction with the CTE of a neighbouring molecule can therefore be excluded.

Interestingly, the majority of shifted signals could be mapped to the substrate binding site (Fig. 4). In addition, atoms for which signals could not be detected, presumably due to exchange broadening, are found in essentially two regions: the active site and the last 12 amino acids of the CTE. The lack of detectable signals for these residues is most likely due to their relaxation properties, whose origin is a transient interaction between the CTE and the active site. The fact that multiple signals for single residues are only observed around proline residues puts the time scale(s) of
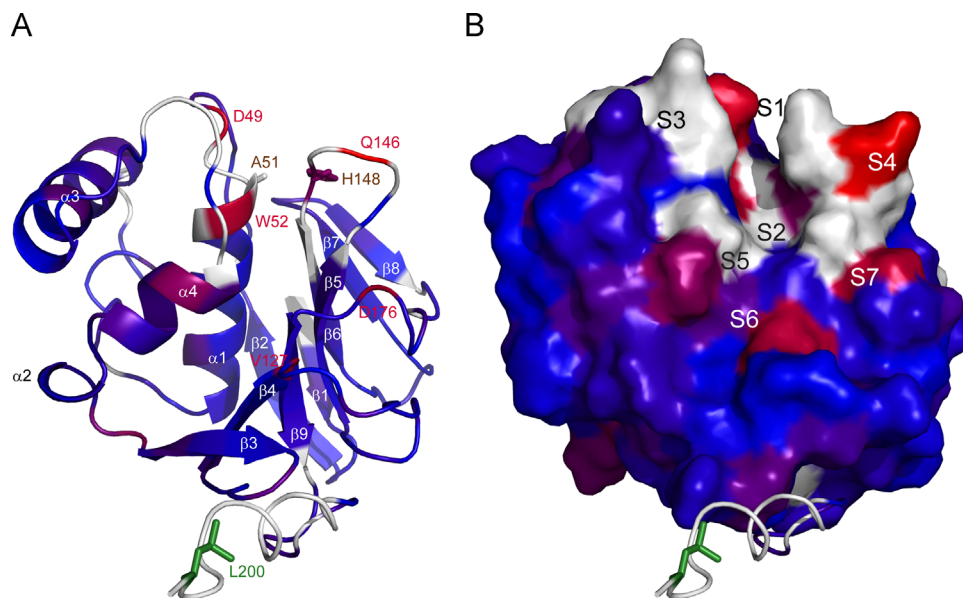
Fig. 4. Location of chemical shift differences between Lb^{pro} L200F and sLb^{pro} shown on the tertiary structure of Lb^{pro} (PDB ID code 1QOL). (A) Amide shift changes induced by the mutation L200F compared to those of sLb^{pro} are mapped onto their positions in the single molecule of Lb^{pro}. The chemical shift changes are colour-coded and range from low (0 ppm, blue) through medium (purple) to high (> 0.50 ppm, red). The active site residues Cys 51 (mutated to Ala) and His 148 (brown labels) as well as Leu 200 (shown in green), are indicated as sticks. Residues showing the greatest shift changes are labelled. Residues for which no signals could be detected are shown in white. (B) The surface structure of the globular domain (colour coded as in (A)) illustrates that the most prominent shift changes map to the substrate binding cleft. (For interpretation of the references to color in this figure legend, the reader is referred to the web version of this article.)
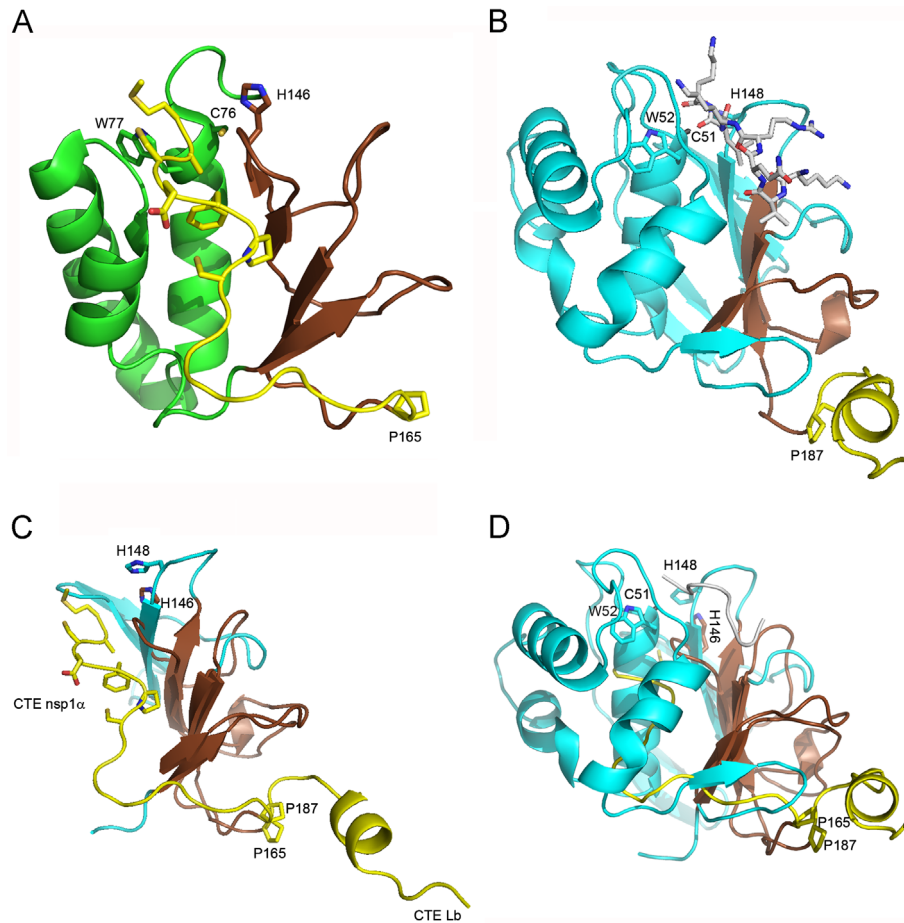
Fig. 5. Comparison and superimposition of nsp1α and Lb^pro. (A) The α-helical domain of nsp1α is coloured green, the β-sheet domain in brown and the CTE (residues 165–180) in yellow. The side-chains of the six most C-terminal residues are shown as sticks. The active site cysteine and histidine side-chains are shown as sticks and labelled as are the tryptophan and proline residues that follow the active site cysteine and lie at the start of the CTE, respectively. (B) The α-helical and β-sheet domains of Lb^pro are coloured blue except for the β-strands that superimpose with nsp1α which are brown. The CTE (187–201) is coloured yellow. In addition, the side-chains of six most C-terminal residues of the CTE of the adjacent molecule in the Lb^pro crystal lattice are shown as grey sticks. The active site cysteine (alanine in black in Lb^pro) and histidine residues are labelled as are the tryptophan and proline residues that follow the active site cysteine and the proline and lie at the start of the CTE, respectively. (C) Superimposition of the C-terminal domains of nsp1α and Lb^pro. For nsp1α, residues 123–180 are shown, for Lb^pro 113–201. Orientation, labelling and colour coding are as in (A) and (B). (D) As (C), except that the N-terminal domain of Lb^pro (in blue) has been introduced and the CTE of nsp1α is shown as a coil. The pdb identifiers are 3IFU and 1QOL (molecules (D) and (B)). (For interpretation of the references to color in this figure legend, the reader is referred to the web version of this article.)

these interactions into the microseconds to milliseconds window. Consequently, many signals will suffer exchange broadening and eventually become undetectable.

Nevertheless, the fact that signals are altered or missing in the substrate binding cleft and the CTE of the same molecule and the presence of a monomeric state, strongly suggests a transient interaction between CTE and active site in an intramolecular manner. It is important for the biological role of Lb^pro that the CTE does not irreversibly remain in the substrate binding cleft, as the enzyme must remain active and its active site must remain accessible in order to cleave its cellular targets such as eIF4GI and eIF4GII (Gradi et al., 2004).

In contrast to Lb^pro, it has been recently shown that the papain-like leader proteinase of PRRSV, nsp1α, undergoes intramolecular self-processing, with the CTE remaining bound to the active site (Sun et al., 2009). To examine why the PRRSV nsp1α proteinase stably binds its CTE as a monomer whereas the FMDV Lb^pro does not, we set out to compare the structures of the two proteinases in more detail than previously done by Sun et al. (Sun et al., 2009). Fig. 5 compares the structures of nsp1α (Fig. 5A) and Lb^pro (Fig. 5B). Both proteins show a typical structure of a papain-like proteinase, with an α-helical and a β-stranded domain; however, the arrangement of the CTEs relative to the globular domain is quite different. For comparison, we have also

depicted the position of the CTE of the adjacent molecule to the FMDV Lb^pro molecule, allowing the position of the substrate bound in an intermolecular reaction to be seen.

To further compare the structures of the two proteinases, we tried to align them using the DaliLite server (Holm and Sander, 1993). However, using the full-length sequences (residues nsp1α 70–180 and Lb^pro 29–201), no appropriate structural alignment could be generated, even when excluding the CTEs of the two proteins (data not shown). We therefore attempted to produce separate alignments of the N- and the C-terminal domains. Again, we were unsuccessful with the N-terminal domains (data not shown). In contrast, the alignment of the C-terminal domains (123–180 and 113–201) showed that three β-strands of the two proteinases were structurally related, as shown in Fig. 5C. Equivalent parts of the proteins (rmsd 3.7 Å on 35 aligned residues) are coloured brown. Furthermore, the superimposition shows that the β-strands (β5 in nsp1α and β9 in Lb^pro) before the start of the respective CTEs are essentially equivalent; consequently, the first four amino acids of the CTEs protrude from their globular domains in a similar orientation (Fig. 5C). The direction of the CTEs then changes at Pro 187 in Lb^pro and Pro 165 in nsp1α. This juxtaposition of the two proline residues supports the idea that Pro 187 is a functionally important residue in the CTE of Lb^pro, as indicated by
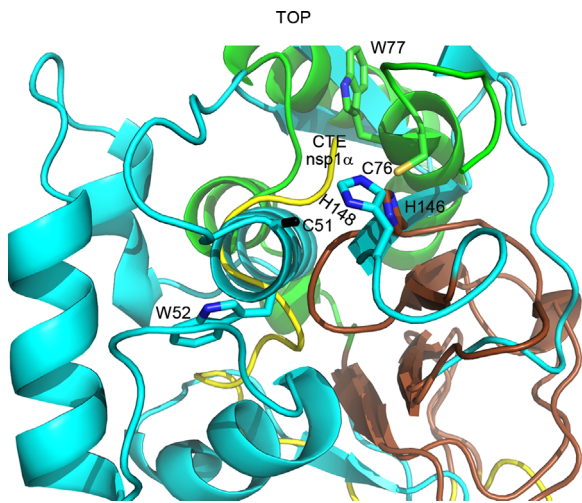
Fig. 6. Relative orientation of the nsp1α and Lb^pro α-helical and β-sheet domains. Superimposition of entire nsp1α and Lb^pro proteins; the orientation is rotated 90° on the *x*-axis compared to Fig. 5 (A) to look down on the active sites. Residues 155–168 (comprising strands β7–β8) of Lb^pro have been omitted for clarity.

its conservation and that it was potentially acting as a 'conformational switch' as indicated by the NMR signal doubling observed for Glu 186 and Leu 188 in Lb^pro.

The first residues of the CTEs of the two proteinases appear therefore to be placed similarly, but the CTE of Lb^pro does not follow that of the nsp1α into the active site of the same molecule. One reason for the differences is the presence of the extra β-sheets in the C-terminal domain of Lb^pro that would clash with a CTE placed in a position analogous to nsp1α. To investigate this further, we then examined the orientation of the α-helical domains of the two proteinases relative to each other. This was done by taking the existing superimposition of the C-terminal domains and adding the N-terminal domain of Lb^pro to that overlay.

Fig. 5D shows the superimposition of the complete FMDV Lb^pro with the C-terminal strands of nsp1α. In this hypothetical arrangement, the trace of the CTE of nsp1α clashes with a region occupied by the N-terminal domain of Lb^pro, further indicating that the self-processing of Lb^pro has to be different from that of nsp1α. This observation implies therefore that the orientation of the N-terminal domains of Lb^pro and nsp1α must be different. Indeed, the superimposition of the complete chains of the two proteinases (viewed from the top, looking down the active site) illustrates that the α-helical domain of nsp1α containing the active site cysteine is rotated about 180° to that of Lb^pro (Fig. 6; compare the positions of the active site cysteines and the adjacent tryptophan residues) so that the two nucleophiles are pointing in the opposite direction. As papain and other relatives such as cathepsin B superimpose in both α-helical and β-sheet domains to Lb^pro, this makes the nsp1α a very unusual enzyme. Compared to the canonical papain-like enzymes (Berti and Storer, 1995; Turk et al., 1997), it appears that the nsp1α is much less compact and the substrate binding area much broader. In addition, the position of the Cys nucleophile relative to that of the catalytic His residue is quite different to that found in the nsp1α. It is tempting to speculate that the reason that the nsp1α forms a stable intramolecular complex with its CTE is to

increase the stability of the globular domain. In contrast, in Lb^pro, the globular domain is stable and active without the CTE, thus allowing it to be released following self-processing.

In conclusion, we provide structural evidence for a mechanism of self-processing of the FMDV Lb^pro that involves a transient intramolecular interaction between the active site of one molecule and its own CTE that is quite different from intramolecular self-processing found in PRRSV nsp1α.

Acknowledgments

References

Berti, P.J., Storer, A.C., 1995. Alignment/phylogeny of the papain superfamily of cysteine proteases. J. Mol. Biol. 246, 273–283.

Cencic, R., Mayer, C., Juliano, M.A., Juliano, L., Konrat, R., Kontaxis, G., Skern, T., 2007. Investigating the substrate specificity and oligomerisation of the leader protease of foot and mouth disease virus using NMR. J. Mol. Biol. 373, 1071–1087.

Delaglio, F., Grzesiek, S., Vuister, G.W., Zhu, G., Pfeifer, J., Bax, A., 1995. NMRPipe: a multidimensional spectral processing system based on UNIX pipes. J. Biomol. NMR 6, 277–293.

DeLano, D.L., 2002. The Pymol Molecular Graphics System. DeLano Scientific, Palo Alto, CA, USA.

Devaney, M.A., Vakharia, V.N., Lloyd, R.E., Ehrenfeld, E., Grubman, M.J., 1988. Leader protein of foot-and-mouth disease virus is required for cleavage of the p220 component of the cap-binding protein complex. J. Virol. 62, 4407–4409.

Glaser, W., Cencic, R., Skern, T., 2001. Foot-and-mouth disease virus leader proteinase: involvement of C-terminal residues in self-processing and cleavage of eIF4GI. J. Biol. Chem. 276, 35473–35481.

Goddard, T., Kneller, D.G., SPARKY 3. University of California, San Francisco, San Francisco.

Gradi, A., Foeger, N., Strong, R., Svitkin, Y.V., Sonenberg, N., Skern, T., Belsham, G.J., 2004. Cleavage of eukaryotic translation initiation factor 4GII within foot-and-mouth disease virus-infected cells: identification of the ʟ-protease cleavage site in vitro. J. Virol. 78, 3271–3278.

Guarne, A., Hampoelz, B., Glaser, W., Carpena, X., Tormo, J., Fita, I., Skern, T., 2000. Structural and biochemical features distinguish the foot-and-mouth disease virus leader proteinase from other papain-like enzymes. J. Mol. Biol. 302, 1227–1240.

Guarne, A., Tormo, J., Kirchweger, R., Pfistermueller, D., Fita, I., Skern, T., 1998. Structure of the foot-and-mouth disease virus leader protease: a papain-like fold adapted for self-processing and eIF4G recognition. EMBO J. 17, 7469–7479.

Holm, L., Sander, C., 1993. Protein structure comparison by alignment of distance matrices. J. Mol. Biol. 233, 123–138.

Kuehnel, E., Cencic, R., Foeger, N., Skern, T., 2004. Foot-and-mouth disease virus leader proteinase: specificity at the P2 and P3 positions and comparison with other papain-like enzymes. Biochemistry (Mosc) 43, 11482–11490.

Mayer, C., Neubauer, D., Nchinda, A.T., Cencic, R., Trompf, K., Skern, T., 2008. Residue L143 of the foot-and-mouth disease virus leader proteinase is a determinant of cleavage specificity. J. Virol. 82, 4656–4659.

Santos, J.A., Gouvea, I.E., Judice, W.A., Izidoro, M.A., Alves, F.M., Melo, R.L., Juliano, M.A., Skern, T., Juliano, L., 2009. Hydrolytic properties and substrate specificity of the foot-and-mouth disease leader protease. Biochemistry (Mosc) 48, 7948–7958.

Sun, Y., Xue, F., Guo, Y., Ma, M., Hao, N., Zhang, X.C., Lou, Z., Li, X., Rao, Z., 2009. Crystal structure of porcine reproductive and respiratory syndrome virus leader protease Nsp1alpha. J. Virol. 83, 10931–10940.

Tang, C., Louis, J.M., Aniana, A., Suh, J.Y., Clore, G.M., 2008. Visualizing transient events in amino-terminal autoprocessing of HIV-1 protease. Nature 455, 693–696.

Turk, B., Turk, V., Turk, D., 1997. Structural and functional aspects of papain-like cysteine proteinases and their protein inhibitors. Biol. Chem. 378, 141–150.

Xue, F., Sun, Y., Yan, L., Zhao, C., Chen, J., Bartlam, M., Li, X., Lou, Z., Rao, Z., 2010. The crystal structure of porcine reproductive and respiratory syndrome virus nonstructural protein Nsp1beta reveals a novel metal-dependent nuclease. J. Virol. 84, 6461–6471.